ELSEVIER

Contents lists available at ScienceDirect

### **Chemical Engineering Science**

journal homepage: www.elsevier.com/locate/ces



## On the use of a powder rheometer to probe defluidization of cohesive particles



Ipsita Mishra a, Peiyuan Liu a, Abhishek Shetty b, Christine M. Hrenya a,\*

- <sup>a</sup> Department of Chemical and Biological Engineering, University of Colorado Boulder, Boulder, CO 80303, United States
- <sup>b</sup> Rheology Department, Anton Paar USA, Inc, 10215 Timber Ridge Drive, Ashland, VA 23005, United States

#### HIGHLIGHTS

- Defluidization experiments in a powder rheometer for fine glass particles are reported.
- An impeller at a sufficiently high rotation speed is shown to mitigate channeling.
- The defluidization measurements are shown to be independent of bed diameter and height.
- Sensitivity of the measurements to the impeller rotation speed is reported.
- Torque is identified as an alternative to pressure-drop to characterize defluidization.

#### ARTICLE INFO

# Article history: Received 15 July 2019 Received in revised form 3 December 2019 Accepted 8 December 2019 Available online 9 December 2019

#### ABSTRACT

Inter-particle cohesion plays an important role in various industrial unit operations. Recently, particle defluidization was identified as a bulk measurement that can be used to extract inter-particle cohesion (Liu et al., 2018). This method requires direct-coupling of experimental, "standard" defluidization curves (pressure-drop vs. gas velocity) with discrete-element-method (DEM) simulations; "standard" refers to defluidization without channeling. Hence, the method is not readily applicable to highly-cohesive (Group C) particles that exhibit channeling. In this work, we obtain standard-defluidization-curves for Group C particles using a rheometer with a rotating impeller. Then, we confirm that the measurements from the rheometer are system-size-independent, thereby ensuring the feasibility of direct-coupling of the experiments with smaller DEM simulations. Furthermore, we show that the torque required to rotate the impeller may provide an alternative to the pressure-drop to characterize particle defluidization. Finally, we show that the extracted characteristic-velocities from these experiments may provide a relative-gauge for particle-level cohesion.

© 2019 Elsevier Ltd. All rights reserved.

#### 1. Introduction

Cohesive particles are found in a wide range of industrial processes, such as mixing, sedimentation, fluidization, and granulation, to name a few. The complex behavior of cohesive-particle systems has triggered interest from both the physics and engineering communities, e.g., (Castellanos et al., 1999; Seville et al., 2000; McCarthy, 2003; Tomas, 2004; Herminghaus, 2005; Mitarai and Nori, 2007; Rognon et al., 2007; Boyce, 2018). Numerous previous works have reported that inter-particle cohesion leads to porous packing (Yang et al., 2003; Valverde and Castellanos, 2007), poor fluidization (Geldart, 1973; Rhodes et al., 2001), avalanching flow (Tegzes et al., 2002; Freyssingeas et al., 2011), and formation of agglomerates in the riser (McMillan et al., 2013; Liu and Hrenya,

2018). Therefore, to accurately predict the complex behavior of many-particle systems (macro-scale), an understanding of interparticle cohesion (micro-scale) is crucial (Forsyth et al., 2002; Castellanos, 2005; Luding, 2005; Hou et al., 2012; Shabanian and Chaouki, 2015; Cocco et al., 2017).

To predict particle-level cohesion, both direct and indirect experimental methods have been explored in prior works. For example, atomic force microscopy (AFM) has been used to directly measure the cohesive force (pull-off force) between two particles (Ducker et al., 1991; Larson et al., 1993; Claesson et al., 1996; Jones et al., 2003; Butt et al., 2005). However, the direct measurement is not easy to perform since it requires two particles to align perfectly so that frictional (tangential) interactions can be eliminated; otherwise, the frictional force will add to the normal (cohesive) force in a manner that is hard to quantify (Fernandez et al., 2015). Additionally, to obtain a cohesive force vs. distance curve, the non-contact forces (when surfaces are separated by small,

<sup>\*</sup> Corresponding author.

E-mail address: hrenya@colorado.edu (C.M. Hrenya).

but non-zero distances) are even more difficult to resolve (Cappella and Dietler, 1999). The aforementioned scenarios are further complicated for non-spherical particles.

As an alternative to the direct measurement of cohesive forces, indirect measurements have also been pursued via different force models. Cohesion is highly sensitive to particle-particle separation distance, which is controlled by surface roughness (Liu et al., 2016b), and thus state-of-the-art force models incorporate roughness as a key input parameter. Two such prominent models have been proposed by Rumpf (1990) and Rabinovich et al. (2000a; 2000b). The Rumpf model assumes the asperities to be hemispheric, whereas the Rabinovich et al. model treats asperities as submerged spheres, and also allows for separating particle roughness into two length scales (large-scale and small-scale). The implementation of these models requires precise measurement of roughness from the surface maps of particles. Although obtaining AFM surface maps is relatively straightforward compared to the direct measurement of pull-off forces via AFM, translating these surface roughness maps into input parameters for the cohesion models comes with challenges. Rabinovich et al. (2000a) proposed a method to quantify the measured asperity height and radius from the AFM surface maps in terms of wavelength and root-mean-square average height (roughness parameters). The force predictions using the Rabinovich et al. model compared well with experimental measurements - with a factor of two underprediction - compared to past attempts. More recently, LaMarche et al.(2017a) identified two artifacts - Gibbs (ringing) and "atomic-scale-noise" - that occurred during the extraction of roughness parameters; the methods proposed to account for these artifacts effectively eliminated the factor-of-two mismatch. Altogether, the state-of-the-art force models have vastly improved over the last several decades. However, the applicability of the aforementioned models is limited to spherical particles with no more than two distinct scales of roughness and a single point of contact. Therefore, the approach cannot be easily extended to a wide range of industrial materials - e.g., non-spheres with more than one point of contact.

Another approach to predicting cohesion via indirect measurements involves the numerical integration of van der Waals forces between surfaces (i.e., summing up all the forces from pairwise molecular interactions across the two surfaces). To implement this method, the measured surface maps are reproduced via discretized meshes, and van der Waals forces between the discretized meshes of the two surfaces are determined using the Hamaker model (Cooper et al., 2001; Eichenlaub et al., 2004; Jaiswal et al., 2009; Chen et al., 2010). This method shows good quantitative agreement between predicted and measured forces (Jaiswal et al., 2009). Although this numerical approach is useful to predict cohesive forces for non-spherical particles as well as particles with multiple contacts, the prediction is limited to a specific orientation of particles, and the distribution of particle-contact orientations in a flowing system is difficult to estimate a priori.

Overall, estimating particle-level cohesion from AFM, either directly or indirectly via surface maps, is complex and inefficient to carry out in an industrial setting where feedstock as well as operating conditions (e.g., humidity) can change frequently. Therefore, identifying a quick and inexpensive way to estimate interparticle cohesion from straightforward bulk measurements is highly desirable.

In an attempt to develop a method to extract particle-level cohesion from bulk measurements, Liu et al. (2018) recently proposed a simplified "square-force" cohesion model. The parameters for this model are the maximum cohesive force ( $F_{c,max}$ ) and a cutoff distance ( $D_c$ ), above which the constant cohesion force vanishes. The model is motivated by recent work carried out by

LaMarche et al. [Towards a universal description of cohesiveparticle flows (under review)], which shows that the effect of cohesion on particulate systems can be described by two key quantities: a maximum cohesive force  $(F_{c,max})$  and a critical cohesive energy. In denser systems where sustained multi-particle contacts occur, the maximum cohesive force dictates the particle motion; in relatively dilute systems where rapid collisions dominate, the critical cohesive energy (kinetic energy demarcating agglomeration and de-agglomeration) dictates the ensuing motion. Using discrete element method (DEM) simulations, Liu et al. (2018) isolated the corresponding force-dominated and energy-dominated regimes during defluidization and then showed that the parameters for the square-force cohesion model can be extracted from "standard" defluidization curves, where "standard" refers to the absence of channeling and/or cracking - i.e., no large and erratic fluctuations in the defluidization curve. Since the square-force model relies on bulk measurements to extract cohesion parameter, this model provides a straightforward method to estimate inter-particle cohesion compared to the direct and indirect particle-level measurements discussed earlier.

Overall, to estimate inter-particle cohesion from bulk measurements, a basic requirement is standard defluidization curves for the particles of interest. These curves are easy to obtain for the particles categorized as mildly-cohesive (Geldart Group A), but not so for highly-cohesive ones (Geldart Group C) due to the formation of channels and cracks (Geldart, 1973; Geldart et al., 1984). Generally, the fully-fluidized state of the particles is the state when the normalized pressure drop ( $\Delta P^*$ ) across the particle bed becomes unity, where  $\Delta P^* = \frac{\Delta P}{W/A}$ ;  $\Delta P$  is the pressure drop across the particle bed, Wis the weight of the particles, and A is the bed correctional area. In systems with channeling,  $\Delta P^*$  usually does not reach unity when fluidized and erratic defluidization curves are instead observed (Wang et al., 1998). Thus, the main objective of the present work is to identify a robust system that can provide standard defluidization curves for Group C particles. These particles will require additional energy to eliminate channeling and reach the fully-fluidized state ( $\Delta P^* = 1$ ). In this work, a rheometer with a rotating impeller is used to provide additional energy that assists in the fluidization. Rheometers have been used in previous work to study flowability or to determine the yield locus of particles under different consolidation stress (Freeman, 2007; Bharadwaj et al., 2010; Leturia et al., 2014; Salehi et al., 2017a; Salehi et al., 2017b). Furthermore, since DEM simulations are limited by system size, the defluidization measurements from the rheometer are explored in this work for system size independence to ensure the future feasibility of direct comparison with DEM simulations (e.g., to extract the parameters of the square-force model). Finally, besides the conventional pressure drop profile, the rheometer also provides a profile for the torque required to rotate the impeller inside the particle bed. The torque, another straightforward measurement from the defluidization experiments performed in the rheometer, can be useful to gain insights about the particle-level cohesion.

#### 2. Experiments

#### 2.1. Particles

Soda-lime glass spheres obtained from Mo-Sci Corp were used in all experiments. To obtain a relatively monodisperse distribution, particles were sieved using standard sieves. Five different size ranges of glass particles were used in the experiments – 10–20  $\mu$ m ( $d_{avg}$  = 15  $\mu$ m; Group C), 20–38  $\mu$ m ( $d_{avg}$  = 29  $\mu$ m; Group A), 45–53  $\mu$ m ( $d_{avg}$  = 49  $\mu$ m; Group A), 63–75  $\mu$ m ( $d_{avg}$  = 69  $\mu$ m; Group A), and 150–180  $\mu$ m ( $d_{avg}$  = 165  $\mu$ m; Group B). The average

diameter ( $d_{avg}$ ), determined as the middle of the sieve size range, is used in text below to refer to a given sieve range. The material density of the soda-lime glass particles was obtained from the values supplied by the manufacturer (i.e., 2500 kg/m³). Based upon the given size and density, particles are classified into Group A, Group B, and Group C using Geldart's chart (Geldart, 1973). Detailed characterizations of these particles are given in LaMarche et al. (2017b).

#### 2.2. Experimental apparatus

An Anton Paar rheometer (MCR 502 series), shown in Fig. 1, was used in this work. The fluidized bed portion of the rheometer (powder cell), is a 0.05 m internal-diameter glass cylinder with an indium-tin-oxide coating intended to reduce electrostatic effects. Additionally, the whole system is grounded in order to minimize electrostatic effects. Compressed air at local atmospheric conditions, namely a density of 0.97 kg/m<sup>3</sup> and viscosity of  $1.83 \times 10^{-5}$  Pa s, was used as the fluidizing gas. A Burkert mass flow meter was used to regulate gas flow to the bottom of the powder cell (0-15 L/min range mass flow meter for the 165 μm particles, and 0-5 L/min for all other particles). Before entering the rheometer, the compressed air supply in the lab was passed through a series of moisture traps in order to avoid added cohesion due to capillary condensation (LaMarche et al., 2016). A Duran Group sintered glass porous plate with a diameter of 55 mm, a thickness of 4.5 mm, and an average porosity of 15 µm was used as the gas distributor at the bottom of the powder cell for 165 µm, 69 µm, 49 µm, and 29 µm particles. For 15 µm particles, a Mott Corp sintered stainless steel porous plate with a diameter of 55 mm, a thickness of 1.19 mm and an average porosity of 0.5 µm was used since these particles have a smaller diameter than the average pore size of the distributor plate. In the experiments, the pressure drop across the distributor plate was always higher than 0.2 times the pressure drop across the particle bed, which ensures uniform distribution of the gas entering the powder cell (Kunii and Levenspiel, 1991). A Keller pressure transducer is located just above the porous plate to record the absolute pressure.

The rheometer is supplied with impellers of different geometries, such as double-blade, cylindrical, etc. For all the experiments carried out in this work, the double-blade impeller was used, as shown in Fig. 1a. This impeller has a 150 mm long stem, and a

blade with a total (tip-to-tip) width of 36 mm, a height of 10 mm, and a thickness of 1 mm. The rheometer is also equipped with a torque sensor, which measures the torque required to rotate the impeller at a specific rotation rate, and is capable of measuring a wide range of torque values ( $10^{-8}$  – 0.23 N m). The impeller rotation speed can be varied between 0 and 3000 rotations per minute (rpm). The rheometer is operated via built-in software that allows the user to program the desired sequence of operations and data collection.

#### 2.3. Experimental method

For the defluidization experiments, a minimum of 80 ml of particles (corresponding to a static bed height of 3.7 cm) were loaded into the powder cell (with the rheometer open as shown in Fig. 1a) so that the impeller blades remain completely covered once immersed in the particle bed. After loading the particles, the rheometer is closed (Fig. 1b) where the impeller maintains a distance of 10 mm with the bottom of the powder cell. The bed was initialized by maintaining the gas velocity (U) at a maximum value (dependent on particle size), which ensures a fully fluidized state of the particles ( $\Delta P^* = 1$ ). U was then decreased incrementally by 0.045 cm/s, and the absolute pressure at each U was measured just above the distributor plate. The absolute pressure was measured first with an empty column and then again after the particles were loaded. The difference between these two measurements is equivalent to the pressure drop  $(\Delta P)$  across the particle bed. Additionally, the torque  $(\tau)$  required to rotate the impeller inside the particle bed was measured at each *U*.

After each reduction in the gas velocity, the particle bed requires sufficient time to reach a steady state. To illustrate the sensitivity of the measurements to wait times between subsequent gas velocities, see Fig. 2 for 29  $\mu$ m particles. If the particle suspension is not given sufficient time to reach a steady state after reducing the velocity, the fluidizing gas continues to escape through the bed (Chirone, 2018), which results in a higher  $\Delta P^*$ ; see, for example, Fig. 2a for 0.5 s wait times. Moreover, the solid volume fraction of the particle bed will be smaller (i.e., a more expanded bed) compared to the steady state. Correspondingly, the measured torque values are smaller at lower waiting times (Fig. 2b), as the torque required to rotate the impeller is proportional to the solid volume

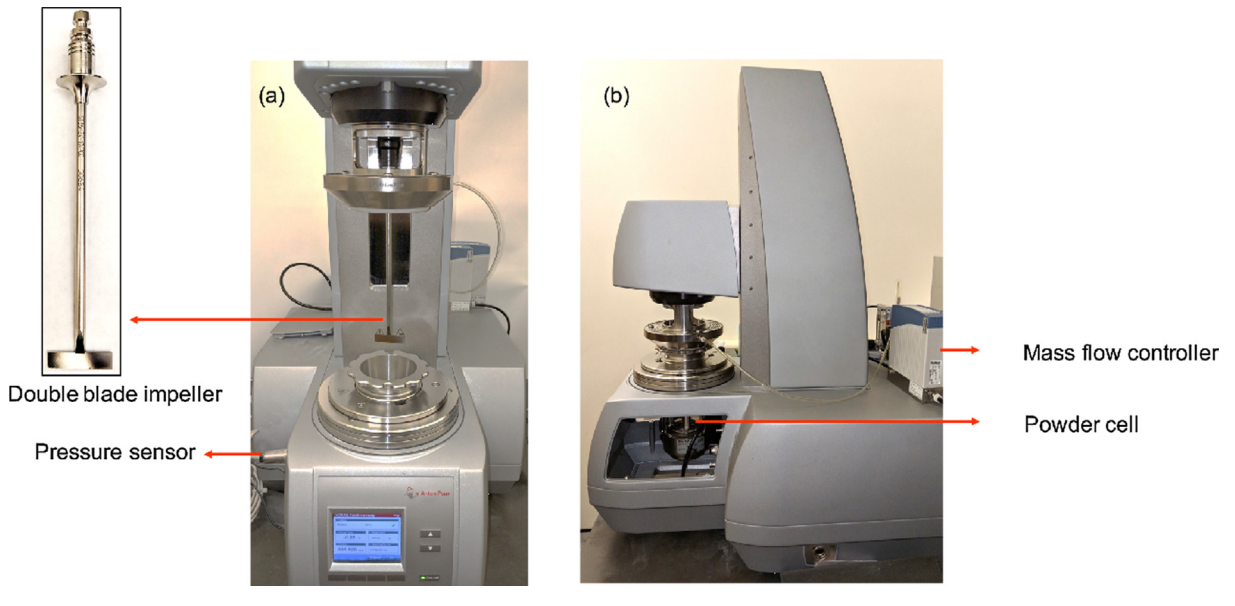
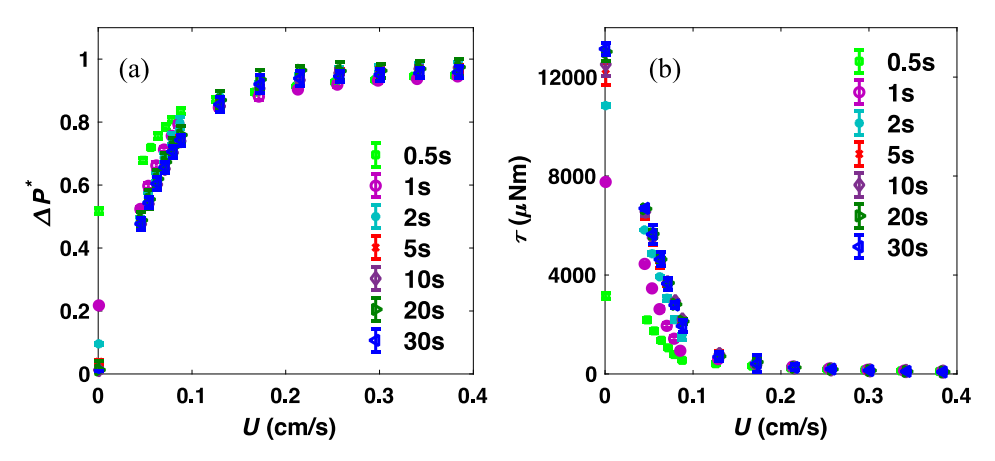


Fig. 1. (a) Front view of the rheometer (open) with the double-blade impeller and (b) side view (closed).



**Fig. 2.** Defluidization curves for (a) pressure drop and (b) torque using 29 μm particles (data points at each gas velocity overlap after 5 s, and hence the system is considered at pseudo-steady-state after 5 s.). The error bars represent 95% confidence interval based upon six different trials.

fraction of the bed (Bruni et al., 2007). Finally, it is found that the time required to reach a steady state depends on the particle size (results not shown for the sake of brevity). A possible explanation for this behavior is that with decreasing particle size, the relative impact of van der Waals cohesion increases (Molerus, 1982; Visser, 1989). As the influence of inter-particle cohesion increases, more time is required to attain a steady particle packing (Yang et al., 2003). For 69 µm particles, the pressure drop and torque measurements at each gas velocity are statistically the same after 1 s of waiting period between each reduction of the gas velocity, whereas for 29 µm particles, the values at each gas velocity are statistically the same only after 5 s, as shown in Fig. 2. The time required for the bed to reach a steady state at each gas velocity further increases to 10 s for 15 µm particles. Therefore, for accurate measurements, the gas flow rate for each particle size examined was held constant for 30 s; the pressure and torque data reported below represent average measurements over the last 20 s of each 30 s interval.

#### 3. Results and discussion

#### 3.1. Defluidization of mildly-cohesive (group A) particles

To first carry out a qualitative assessment of particle defluidization in the rheometer, defluidization results for mildly-cohesive particles (Group A) are obtained. Group A particles are chosen for

the purpose of comparison with a conventional fluidized bed since these particles are easily fluidizable, whereas more cohesive particles (Group C) would exhibit channeling in a conventional bed.

Following the experimental procedure given in Section 2.3, the normalized pressure drop  $(\Delta P^*)$  vs. gas velocity (U) profiles are obtained for three sets of mildly-cohesive, or Group A, particles (69 μm, 49 μm, 29 μm); see Fig. 3a. The fully-fluidized state achieved at higher velocities is indicated by  $\Delta P^* \approx 1$  - i.e., the weight of the particles is borne completely by the drag forces exerted by the fluidizing gas. During defluidization, with the reduction in gas velocity,  $\Delta P^*$  gradually decreases, indicating particles are transitioning from a fully-fluidized state to a static (packed bed) state. During this transition,  $\Delta P^*$  varies non-linearly with the gas velocity (Fig. 3a), which is due to the formation of a partially-fluidized regime that can be attributed to the effect of inter-particle cohesion (Valverde et al., 2003; Tsinontides and Jackson, 2006; LaMarche et al., 2016). As the particle size decreases, the relative impact of inter-particle cohesion increases (Molerus, 1982; Visser, 1989). Thus, the curvature of the pressure profile, which is associated with the partially fluidized regime, is more prominent for the case of 29 µm particles (Fig. 3a), which is consistent with previous observations from a conventional fluidized bed (LaMarche et al., 2017b).

To characterize the defluidization of the particles, the complete fluidization velocity  $(U_{cf})$  is extracted from the curves shown in Fig. 3a.  $U_{cf}$  is defined as the gas velocity at which the drag force

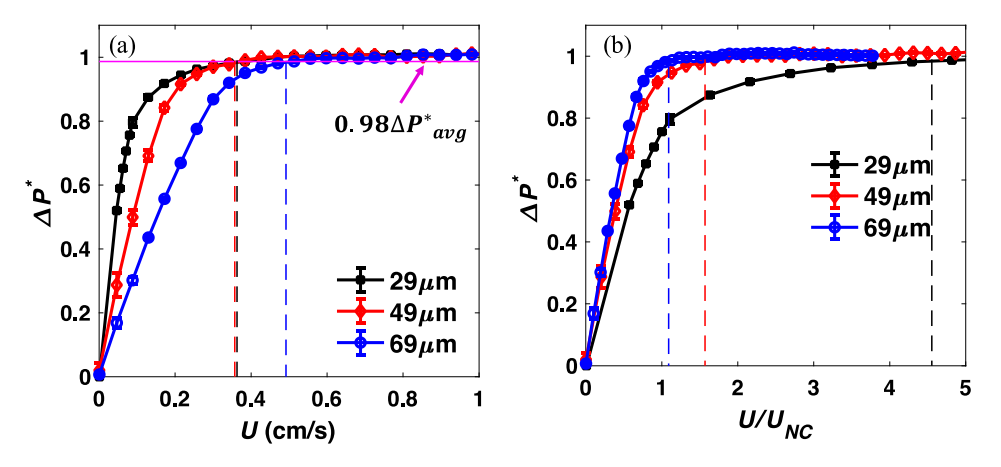


**Fig. 3.** (a) Defluidization curves ( $\Delta P^*$  vs. U) for three different size particles obtained from the rheometer at an impeller speed of 8 rpm. Dotted lines represent corresponding  $U_{cf}$ .(b) defluidization curves where the gas velocity is non-dimensionalized by the corresponding non-cohesive characteristic velocity ( $U_{NC}$ ) to demonstrate the deviation of  $U_{cf}/U_{NC}$  from unity depending on the relative impact of cohesion. Dotted lines represent corresponding  $U_{cf}/U_{NC}$ .

can no longer support the weight of the particles, thereby indicating the onset of defluidization. In this work, the gas velocity at which the pressure drop falls below 98% of the averaged pressure drop at full fluidization ( $\Delta P^*_{avg}$ ) is treated as  $U_{cf}$  (Liu et al., 2016a; LaMarche et al., 2017b), as shown by the vertical lines in Fig. 3a. With a decrease in particle size, a smaller drag force is required to fully fluidize the particles. However, a nonmonotonic trend is observed in the extracted  $U_{cf}$  values for the three different size glass particles, i.e.,  $U_{cf}$  for 29  $\mu$ m is slightly higher than that for 49 µm (Fig. 3a). An explanation for this behavior may arise from the competitive effects of the particles weight and the relative impact of inter-particle cohesion. Due to a higher influence of inter-particle cohesion for 29 µm particles (Molerus, 1982; Visser, 1989), the drag force required to keep these particles in the fluidized state increases, and thus the extracted  $U_{cf}$  is higher than that for the 49  $\mu$ m particles. To further confirm the increase in the relative impact of cohesion with decreasing particle size, the extracted  $U_{cf}$  values are compared with the corresponding noncohesive characteristic velocity ( $U_{NC}$ ).  $U_{NC}$  was calculated using the Carman-Kozeny pressure drop correlation (Carman, 1937) with a solid volume fraction ( $\varepsilon_s$ ) of 0.58 (i.e., non-cohesive  $\varepsilon_s$ ). The above correlation provides the gas velocity corresponding to  $\Delta P^* = 1$  in the absence of particle-particle cohesion. As illustrated in Fig. 3b, the deviation of  $U_{cf}/U_{NC}$  from unity is the largest for 29 µm particles, shown by the dotted line on x-axis, thereby confirming that the relative impact of cohesion is greater for these particles. Hence, the percentage deviation of the extracted  $U_{cf}$  from the corresponding  $U_{NC}$  may serve as a relative gauge for estimating the cohesion level between particles.

#### 3.2. Assessment of the effect of system size

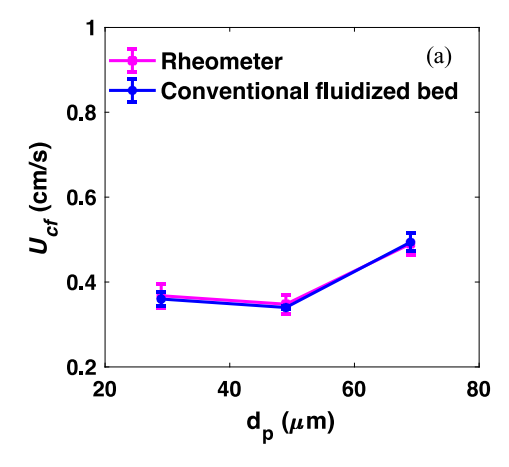
One of the objectives of the current work is to identify an experimental set up that can be directly compared with DEM simulations in order to estimate particle-level cohesion (discussed in Section 1). Since DEM simulations are computationally limited to smaller systems (e.g., Alobaid et al., 2014; Amritkar et al., 2014; Liu and Hrenya, 2014), the effect of system size (i.e., bed diameter and static bed height) on the rheometer measurements should be explored. Ideally, both the experiments and DEM simulations should be system-size independent in order to make an applesto-apples comparison between the two.

To test the sensitivity of the defluidization results from the rheometer to the bed diameter, the results obtained from the rheometer and a conventional fluidized bed with a larger diameter were compared. This approach is an alternative to changing the

diameter of the powder cell, which is difficult to achieve. A detailed description of the fluidized bed is given in Chew et al. (2010), and the experimental procedure is explained by LaMarche et al. (2017b). As depicted in Fig. 4a, the comparison between the rheometer and the fluidized bed experiments shows quantitative agreement for  $U_{cf}$ . The diameter of the rheometer (5 cm) is much smaller than the diameter of the fluidized bed (18.4 cm), thereby providing evidence that the  $U_{cf}$  obtained from the rheometer is not sensitive to the bed diameter. The bed diameter determines the role of wall effects (e.g., particle-wall friction) on bulk particle behavior (fluidization/defluidization) (Loezos et al., 2002; Tsinontides and Jackson, 2006; Li et al., 2012). The insensitivity of  $U_{cf}$  to the bed diameter (Fig. 4a) indicates that the wall effects (particle-wall friction and particle-distributor cohesion) are negligible in the rheometer, which is consistent with previous defluidization results obtained from conventional fluidized beds for similar bed-to-particle diameter ratios considered in this work (Liu et al., 2008; LaMarche et al., 2015).

The next step for confirming system size independence is to probe the effect of the static bed height in the rheometer on the extracted  $U_{cf}$ . From the DEM simulations of a conventional fluidized bed, Liu et al. (2016a) found that the  $U_{cf}$  for cohesive particles becomes independent of static bed height above a certain limit (1.2cm). In this work, we maintain a static bed height of at least 3.7cm in the rheometer, which exceeds the aforementioned limit. As shown in Fig. 4b, the  $U_{cf}$  obtained from defluidization experiments in the rheometer is indeed insensitive to static beds above such heights.

It is worth noting that in the DEM simulations of conventional fluidized beds,  $U_{cf}$  has been found to be independent of bed height when using the actual Young's modulus for the particles (Liu et al., 2016a). However, using a realistic value of Young's modulus for the particle size range considered here leads to high computational overhead (Liu and Hrenya, 2014). Therefore, to decrease the computational time, DEM simulations are commonly carried out with artificially softened particles, i.e., using a Young's modulus smaller than the true value (Mikami et al., 1998; Di Maio and Di Renzo, 2004; Stevens and Hrenya, 2005; Müller et al., 2008). On the other hand, previous simulations of cohesive particles have shown that the sensitivity of  $U_{cf}$  to bed height increases at smaller values of Young's modulus due to the change in bed porosity with bed height (Liu et al., 2016a). In particular, altering bed height affects solid compression; an increase in solid compression leads to a decrease in bed porosity, which is more pronounced for particles with a lower Young's modulus, and results in a smaller  $U_{cf}$ . Unlike a conventional fluidized bed, however, defluidization experiments



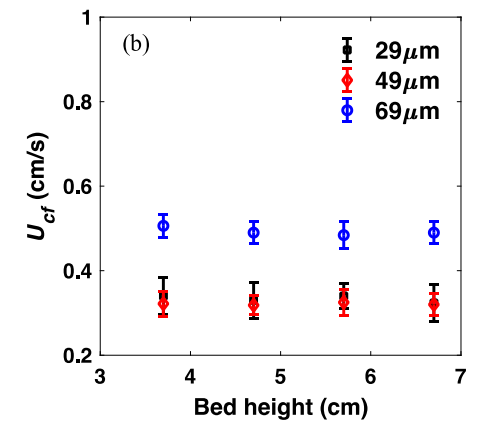


**Fig. 4.** (a) Comparison of  $U_{cf}$  obtained from the rheometer and the conventional fluidized bed with a larger bed diameter, and (b) effect of static bed height on  $U_{cf}$  in the rheometer. The error bars represent the 95% confidence interval based upon six different trials.

carried in the rheometer include a rotating impeller. The rotating impeller keeps the particles well mixed, which may lead to a more uniform local porosity distribution – i.e., minimizing the effect of compression on bed porosity in the rheometer compared to a conventionally fluidized bed. Hence, using a small Young's modulus or a small bed height with actual Young's modulus in DEM simulations of defluidization in the rheometer may be possible without sacrificing accuracy (i.e., if results are insensitive to bed height); admittedly, this possibility needs to be confirmed via DEM simulations, which is outside the scope of the current work.

Overall, experiments with Group A particles establish the insensitivity of  $U_{cf}$  in the rheometer to bed diameter and static bed height. Similar to the above two parameters, the effect of the impeller rotation rate, an inherent system parameter for the rheometer, on particle defluidization is explored, as discussed next.

#### 3.3. Effect of rotation speed of the impeller

For the mildly-cohesive (Group A: 69  $\mu$ m, 49  $\mu$ m, and 29  $\mu$ m) particles,  $U_{cf}$  is found to vary non-monotonically with the rotation speed. As shown in Fig. 5a,  $U_{cf}$  remains constant at relatively low rotation rates (until ~ 40 rpm), and then decreases gradually before a more noticeable increase sets in. The decrease in  $U_{cf}$  is more prominent for 49  $\mu$ m and 29  $\mu$ m particles, for which the impact of inter-particle cohesion is higher compared to 69  $\mu$ m. A plausible explanation for this behavior is that as the rotation speed increases, the impact velocity between a pair of particles just prior to collision increases (presumably near the critical impact velocity

that demarcates agglomeration vs. breakup), thereby enhancing the breakage of the cohesive agglomerates, resulting in a lower  $U_{cf}$ . Consistent with this physical picture, we expect the decreasing trend in  $U_{cf}$  to further diminish when the impact of cohesion decreases. As a check to this hypothesis, the effect of rotation speed on  $U_{cf}$  was explored for 165  $\mu$ m particles (Geldart Group B) where the influence of cohesion due to van der Waals forces is negligible (Molerus, 1982). As shown in Fig. 5b, the overlapping error bars indicate that the  $U_{cf}$  for 165  $\mu$ m particles does not change significantly with the rotation speed until an increase is observed at  $\sim$ 160 rpm, which is consistent with the above hypothesis.

With increase in the rotation speed beyond  $\sim 160$  rpm,  $U_{cf}$ increases for particles of all sizes (Fig. 5a and b). A possible explanation for this behavior may stem from the competitive effects of centrifugal and gravitational accelerations. More specifically, the ratio of the accelerations is expressed by the Froude number ( $Fr = \omega^2 r/g$ , where  $\omega$  is the angular velocity of the impeller, r is the radius of the impeller, and g is the gravitational acceleration). At higher rotation speeds, Fr becomes greater than unity, indicating that the centrifugal acceleration dominates over gravitational acceleration. As a result, particles are pushed more towards the wall, and the normal force on the wall (due to particle-wall contacts) increases. An increase in the normal force on the wall will lead to higher particle-wall frictional forces, thereby requiring a higher drag force (and correspondingly a higher gas velocity) to hold the particles in the fully fluidized state. Consequently, when Fr is greater than unity,  $U_{cf}$  increases with the rotation speed of the impeller, as shown in Fig. 5c. Moreover, in this centrifugal-dominated region

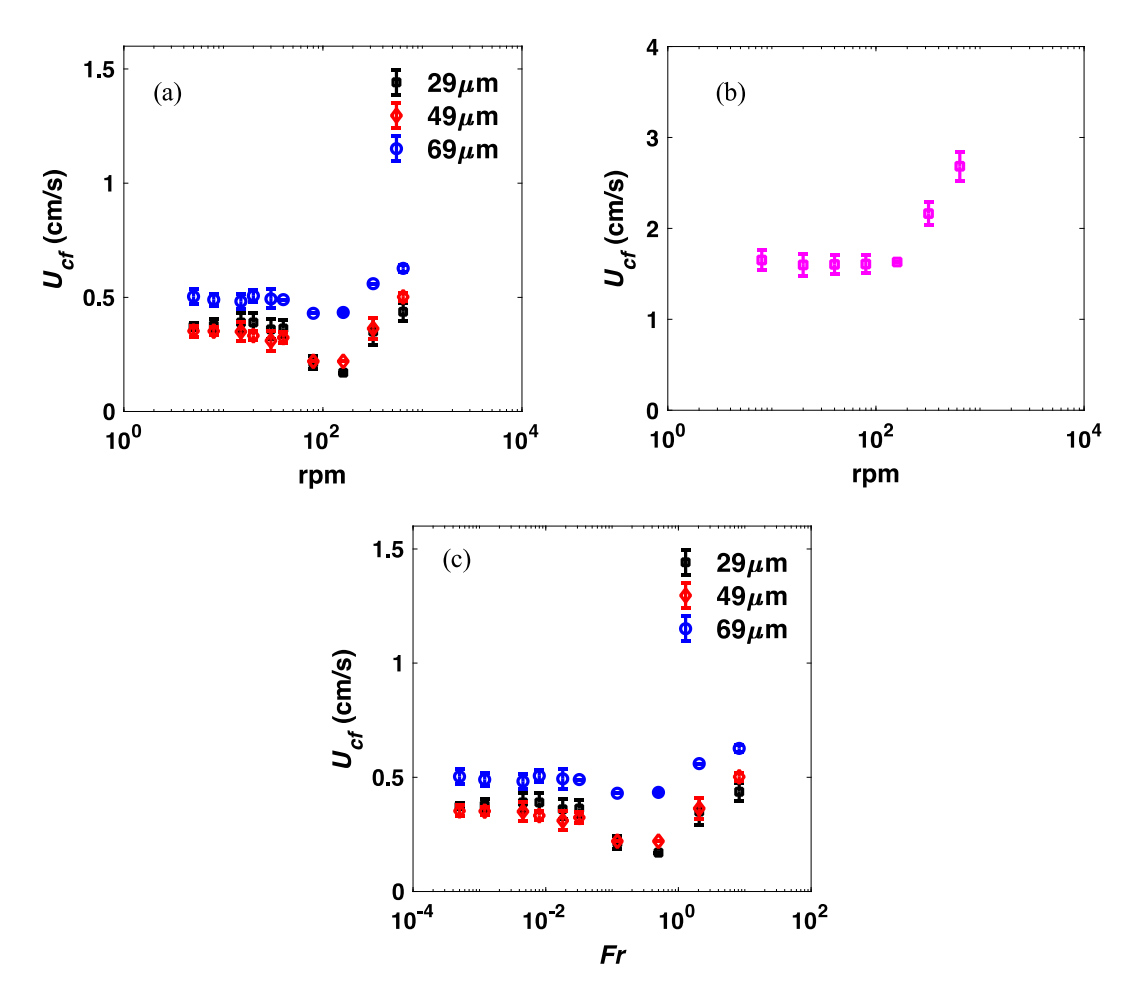


Fig. 5. Sensitivity of  $U_{cf}$  to rotation speed of the impeller (a) mildly-cohesive particles (b) non-cohesive particles (165  $\mu$ m). (c) Variation of  $U_{cf}$  with Fr. The error bars represent the 95% confidence interval.

(Fr > 1), the role of wall effects becomes important. Furthermore, the wall effects will depend on the system size, analogous to the pressure drop overshoot observed during fluidization (Loezos et al., 2002; Srivastava and Sundaresan, 2002; Xu et al., 2017). Hence, the system size effects for Fr > 1 are worth exploring via DEM in future work.

In sum, the experiments indicate that  $U_{cf}$  is insensitive to bed diameter and static bed height, but is sensitive to the impeller rotation speed over a range of  $U_{cf}$ . Therefore, for the purpose of comparing the  $U_{cf}$  values between the rheometer and data from conventional fluidized beds, the regime where  $U_{cf}$  stays constant with impeller speed should be used. Furthermore, when comparing the rheometer results with small-scale DEM simulations, the rotation speed in the simulations can be chosen from the abovementioned regime (i.e., independent of impeller speed). Alternatively, Fr in the simulations can be matched to that of experiments in the centrifugal-dominated regime (Fr > 1), in order to have a similar effect of the centrifugal forces. The validity of the above needs to be tested in future work.

#### 3.4. Torque measurement from the rheometer

As mentioned in Section 2.2, the rheometer is capable of measuring the torque  $(\tau)$  required to rotate the impeller at a specific rotation speed inside the particle bed. As shown in Fig. 6a-c, at the higher gas velocities associated with the fully-fluidized state,  $\tau$  remains relatively constant (albeit with high fluctuations); at lower velocities,  $\tau$  increases with decreasing gas velocity. The torque required to rotate the impeller inside the particle bed is dictated by the resistance offered by the particles, which in turn is dependent on the stress distribution in the particle bed and thus

inversely proportional to bed porosity (Bruni et al., 2007; Salehi et al., 2017a; Salehi et al., 2017b). In the fully fluidized state (high *U*), low torque values are observed compared to the static (packed bed at low U) state as the particle bed offers a minimal resistance for the impeller rotation because of high bed porosity. With decreasing gas velocity, the bed porosity decreases, and hence an increasing trend in  $\tau$  is observed (Fig. 6). Furthermore, the torque fluctuations in the fully fluidized state (Fig. 6a-c) are clearly observed at low rotation speeds (e.g., 8 rpm). As the rotation speed increases beyond ~ 200 rpm, these fluctuations appear to diminish (see Fig. 6d). In the fluidized state, resistance from the particle bed is minimal, and thus the required torque values are dictated by the impeller rotation speed. Therefore, with increasing rotation speed, the corresponding torque values increase (Fig. 6d), and hence the corresponding error bars (standard deviation), which are of similar magnitude at 8 rpm, become less prominent relative to the absolute torque value. Additionally, note that due to the wide range of values displayed on the y-axis, the torque at U = 0cm/s appears to be the same in Fig. 6a-d, but the absolute values vary depending upon particle size, cohesion level, and the rotation speed.

In previous works, the effect of aeration on torque measurement prior to fluidization has been analyzed in terms of stress distribution in the particle bed (Bruni et al., 2005; Bruni et al., 2007; Salehi et al., 2017b; 2018). In the current work, the focus is on the transition from a fluidized state to a packed-bed state in order to determine a characteristic velocity ( $U_{cf}$ ) for defluidization, which is an important parameter to gauge inter-particle cohesion (Section 3.1). It is worth noting that the determination of  $U_{cf}$  from the pressure drop profile (Section 3.1) inherently depends on the data resolution (LaMarche et al., 2017b), i.e., depending on the precision of the mass flow controller, if the interval (incremental

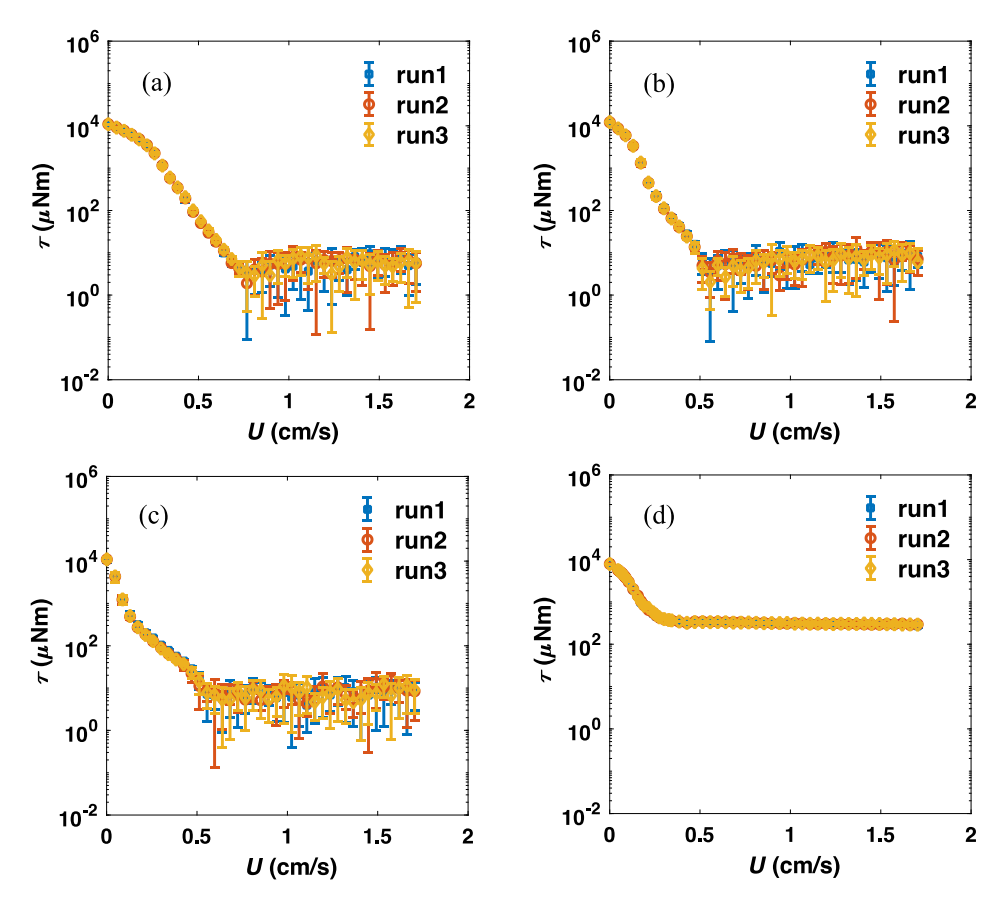
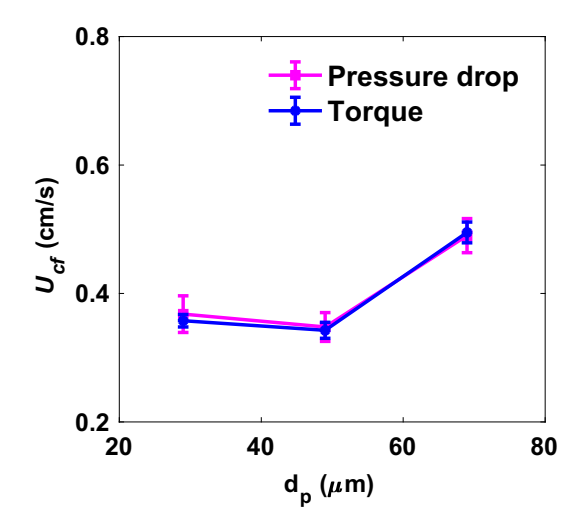


Fig. 6. Torque measurements obtained from the rheometer at 8 rpm rotation speed of the impeller for particles of size: (a) 69  $\mu$ m (b) 49  $\mu$ m (c) 29  $\mu$ m. (d)Torque measurement from the rheometer at 240 rpm rotation speed for 49  $\mu$ m particles. The error bars represent the standard deviations.



**Fig. 7.** Comparison between  $U_{cf}$  obtained from pressure drop and torque profiles. The error bars represent 95% confidence interval based upon six different trials.

value) between the consecutive gas flow rate is changed,  $U_{cf}$  will also change. Furthermore, choosing a cut-off for  $U_{cf}$  is arbitrary, i.e.,  $U_{cf}$  values obtained in this work are based on a 98% cut-off and the values will change slightly if a different cut-off is chosen. To eliminate the dependency of  $U_{cf}$  on data resolution and the arbitrary nature of cut-off values,  $U_{cf}$  is instead determined from the torque profiles as the intersection point of the linearly decreasing regime (obtained by a least-square fit to the data) with the average of the constant- $\tau$  regime. A comparison between  $U_{cf}$  values obtained from the pressure drop and torque profiles are presented in Fig. 7, which indicates  $U_{cf}$  follows the same trend irrespective of the method of extraction. However, by eliminating the dependency on data resolution and arbitrary cut-off values, the error bars associated with  $U_{cf}$  from the torque profiles are smaller than those from the pressure drop profiles for the same number of trials. Hence, given the clear transition from the fluidized state to packed-bed state (Fig. 6), torque profiles provide a good alternative to determine the characteristic velocity of defluidization.

#### 3.5. Defluidization of highly-cohesive (group C) particles

After a careful exploration of the effects of system size and rotation speed of the impeller on defluidization using

mildly-cohesive (Group A) particles, the next step is to investigate the defluidization of cohesive (Group C) particles in the rheometer. At low rotation speeds (e.g., 8 rpm) standard defluidization curves (i.e., defluidization without channeling) are easily obtained for Group A particles (Fig. 3); however, Group C particles fluidize with visible channeling for such rotation speeds in the rheometer. Due to this channeling, the pressure drop across the bed does not support the whole weight of the particle bed, and  $\Delta p^*$  remains below unity even at higher gas velocities (up to 1 cm/s), as depicted in Fig. 8a for 8 rpm. Similarly, the corresponding torque profile (Fig. 8b) does not follow the standard defluidization trend (i.e., does not show distinct decreasing and constant regimes, as discussed in Section 3.4), and the measured torque values are higher for a low impeller rotation speed. In conventional fluidized beds, the channeling exhibited by Group C particles is hard to eliminate. However, in the rheometer, by increasing the impeller rotation speed and thus providing additional energy into the system, channeling can be mitigated. As depicted in Fig. 8, well-behaved defluidization curves (i.e., no signs of channeling) are obtained for the 15 μm particles when the rotation speed is increased to 300 rpm. Hence, with the rheometer, the objective of identifying a robust experimental system to reach standard fluidization of Group C particles is achieved. Furthermore, it is worth noting that due to the challenges involved in obtaining a narrow size distribution for smaller particles (<10 µm) (Rhodes, 2008), the experimental results for Group C particles are presented only for 15 µm particles.

Note that a non-zero pressure drop is observed for the 15 µm particles when the gas velocity drops to zero. A possible reason for this behavior is that the high rotation speed of the impeller (300 rpm) creates a thrust at the bottom of the bed; thus, even at zero gas velocity, momentum transfer occurs from the bottom to the top of the bed, which gives rise to a vertical pressure drop and prevents  $\Delta P^*$  from reaching absolute zero (a similar behavior is also observed for Group A particles when the rotation speed is increased to 300 rpm). It is also worth noting, as previously discussed in Section 3.4, the fluctuations in the torque profile are barely noticeable at high impeller rotation speeds (>200 rpm). Therefore, as shown in Fig. 8b for a rotation speed of 300 rpm, the demarcation in the transition from the fluidized state to packed-bed state is not as sharp as that for Group A particles at lower rotation speeds (Fig. 6a-c). However, the torque profile at the higher impeller speed has distinct constant- $\tau$  and variable- $\tau$ regimes (shown using linear axes in the inset of Fig. 8b), which can still be used as an alternative to the pressure drop profile in order to determine the characteristic velocity for defluidization following the method discussed in Section 3.4. The  $U_{cf}$  values for the

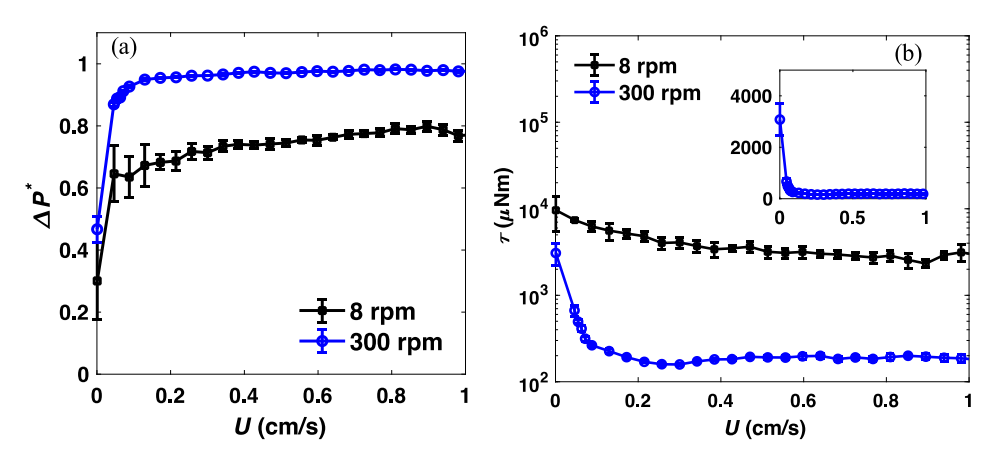


Fig. 8. Defluidization profiles for (a) pressure drop and (b) torque (inset: the y-axis is changed from logarithmic to linear) using 15 μm particles with an impeller rotation speed of 8 rpm and 300 rpm.

15 μm particles that were obtained from the pressure drop and torque profiles are found to be  $0.30 \pm 0.038$  and  $0.28 \pm 0.03$  (the error represents the 95% confidence interval based upon six different trials), respectively. Accordingly, close agreement is found between the values obtained from the two curves. Furthermore, the high rotation speed of the impeller (300 rpm) breaks the cohesive agglomerates, and thus allows the  $U_{cf}$  to be dictated by the particle size (the competitive effects of particle size and inter-particle cohesion is discussed in Section 3.1). Therefore, the  $U_{cf}$  values for 15 μm particles (0.30 ± 0.038) are found to be smaller than that of 29 μm particles (0.35 ± 0.03).

#### 4. Concluding remarks

In the present work, highly-cohesive, Group C particles are successfully fluidized without channeling in a rheometer fluidizing gas and a rotating impeller. The experimental results indicate that the complete fluidization velocity  $(U_{cf})$  is insensitive to bed diameter and static bed height, but shows some sensitivity to impeller rotation speed. More specifically, as the rotation speed increases, U<sub>cf</sub> remains insensitive until a gradual decrease is observed, followed by an increase. This non-monotonic trend can be explained as follows. As impeller speed increases, a corresponding increase in the relative impact velocities of the particles occurs and hence reduced agglomeration occurs, thereby leading to smaller values of  $U_{cf}$  (i.e., closer to the predicted value based on non-cohesive correlations). With a further increase in the rotation speed, the centrifugal acceleration dominates in the system (Fr > 1), which results in an increased effect of particle-wall friction and thus a higher  $U_{cf}$ . Furthermore, torque profiles – the variation in the torque with fluidizing gas velocity - are also obtained from rheometer measurements. The torque profiles provide an alternative way to determine the characteristic velocity for defluidization.

A key benefit of the defluidization experiments performed in the rheometer is that they can be used as a quick gauge for cohesion levels in particles, for example to determine their applicability in different unit operations. Specifically, the difference between the extracted  $U_{cf}$  from the defluidization curves and the corresponding non-cohesive characteristic velocity ( $U_{NC}$ ) (Carman, 1937) provides a straightforward measure of the relative level of inter-particle cohesion. The rheometer measurements are not limited to particles having any particular source of cohesion (e.g., van der Waals force or capillary force), and hence can be used to identify the effects of changes in particle size, shape, or humidity conditions on the cohesion level in a sample using the defluidization curves. Furthermore, compared to conventional fluidized beds, the rheometer is a smaller system which requires less sample material, and thus provides a convenient method to investigate particle flow properties.

Finally, a future goal of this line of inquiry is to obtain a microscale (inter-particle) cohesion model from macro-scale (bulk) measurements. As a first step in this direction, Liu et al. (2018) provided a promising method to determine the cohesion parameters for a square-force model from the standard defluidization curves in conventional fluidized beds; this approach is limited to Group A particles since more cohesive particles will result in channeling. In this work, the standard defluidization curves (i.e., no erratic pressure fluctuations due to channeling) obtained for Group C particles using the rheometer extends the possibility of extracting cohesion parameters for these highly-cohesive particles.

#### **CRediT authorship contribution statement**

**Ipsita Mishra:** Investigation, Formal analysis, Writing - original draft. **Peiyuan Liu:** Conceptualization, Writing - review & editing.

**Abhishek Shetty:** Resources, Writing - review & editing. **Christine M. Hrenya:** Supervision, Funding acquisition, Writing - review & editing.

#### **Declaration of Competing Interest**

The authors declare that they have no known competing financial interests or personal relationships that could have appeared to influence the work reported in this paper.

#### Acknowledgements

The authors are grateful for the financial support provided by the National Science Foundation (CBET-1707046). The authors would also like to gratefully acknowledge Anton Paar for providing the rheometer through their VIP academic research program. The authors thank Michael Molnar, Jing Huang, and Margaret Hwang of Dow for stimulating discussions.

#### References

- Alobaid, F., Baraki, N., Epple, B., 2014. Investigation into improving the efficiency and accuracy of CFD/DEM simulations. Particuology 16, 41–53. https://doi.org/ 10.1016/j.partic.2013.11.004.
- Amritkar, A., Deb, S., Tafti, D., 2014. Efficient parallel CFD-DEM simulations using OpenMP. J. Comput. Phys. 256, 501–519. https://doi.org/10.1016/j.jcp.2013.09.007.
- Bharadwaj, R., Ketterhagen, W.R., Hancock, B.C., 2010. Discrete element simulation study of a Freeman powder rheometer. Chem. Eng. Sci. 65, 5747–5756. https:// doi.org/10.1016/j.ces.2010.04.002.
- Boyce, C.M., 2018. Gas-solid fluidization with liquid bridging: a review from a modeling perspective. Powder Technol. 336, 12–29. https://doi.org/10.1016/j.
- Bruni, G., Barletta, D., Poletto, M., Lettieri, P., 2007. A rheological model for the flowability of aerated fine powders. Chem. Eng. Sci. 62, 397–407. https://doi.org/10.1016/j.ces.2006.08.060.
- Bruni, G., Colafigli, A., Lettieri, P., Elson, T., 2005. Torque measurements in aerated powders using a mechanically stirred fluidized bed rheometer (msFBR). Chem. Eng. Res. Des. 83, 1311–1318. https://doi.org/10.1205/cherd.05092.
- Butt, H.-J., Cappella, B., Kappl, M., 2005. Force measurements with the atomic force microscope: technique, interpretation and applications. Surf. Sci. Rep. 59, 1– 152. https://doi.org/10.1016/j.surfrep.2005.08.003.
- Cappella, B., Dietler, G., 1999. Force-distance curves by atomic force microscopy. Surf. Sci. Rep. 34, 1–104. https://doi.org/10.1016/S0167-5729(99)00003-5.
- Carman, P.C., 1937. Fluid flow through granular beds. Trans. Inst. Chem. Eng. 15, 150–166.
- Castellanos, A., 2005. The relationship between attractive interparticle forces and bulk behaviour in dry and uncharged fine powders. Adv. Phys. 54, 263–376. https://doi.org/10.1080/17461390500402657.
- Castellanos, A., Valverde, J.M., Pérez, A.T., Ramos, A., Watson, P.K., 1999. Flow regimes in fine cohesive powders. Phys. Rev. Lett. 82, 1156–1159. https://doi.org/10.1103/PhysRevLett. 82.1156.
- Chen, Y., Jallo, L., Quintanilla, M.A.S., Dave, R., 2010. Characterization of particle and bulk level cohesion reduction of surface modified fine aluminum powders. Colloids Surf., A 361, 66–80. https://doi.org/10.1016/j.colsurfa.2010.03.015.
- Chew, J.W., Wolz, J.R., Hrenya, C.M., 2010. Axial segregation in bubbling gasfluidized beds with Gaussian and lognormal distributions of Geldart Group B particles. AIChE J. 56, 3049–3061. https://doi.org/10.1002/aic.12219.
- Chirone, R., 2018. A Study of the Effect of Process Conditions on the Fluidization Behaviour of Cohesive Industrial Powders Linked with Rheological Studies, University College London, PhD Thesis.
- Claesson, P.M., Ederth, T., Bergeron, V., Rutland, M.W., 1996. Techniques for measuring surface forces. Adv. Colloid Interface Sci. 67, 119–183. https://doi. org/10.1016/0001-8686(96)00302-8.
- Cocco, R., Fullmer, W.D., Liu, P.Y., Hrenya, C.M., 2017. CFD-DEM: modeling the small to understand the large. Chem. Eng. Prog. 113, 38–45.
- Cooper, K., Gupta, A., Beaudoin, S., 2001. Simulation of the adhesion of particles to surfaces. J. Colloid Interface Sci. 234, 284–292. https://doi.org/10.1006/ icis 2000.7776
- Di Maio, F.P., Di Renzo, A., 2004. Analytical solution for the problem of frictionalelastic collisions of spherical particles using the linear model. Chem. Eng. Sci. 59, 3461–3475. https://doi.org/10.1016/j.ces.2004.05.014.
- Ducker, W.A., Senden, T.J., nature, R.P., 1991, n.d. Direct measurement of colloidal forces using an atomic force microscope. nature.com. doi:10.1111/j.1365-2966.2009.15405.x.
- Eichenlaub, S., Gelb, A., Beaudoin, S., 2004. Roughness models for particle adhesion. J. Colloid Interface Sci. 280, 289–298. https://doi.org/10.1016/j.jcis.2004.08.017.
- Fernandez, N., Cayer-Barrioz, J., Isa, L., Spencer, N.D., 2015. Direct, robust technique for the measurement of friction between microspheres. Langmuir 31, 8809–8817. https://doi.org/10.1021/acs.langmuir.5b01086.

- Forsyth, A.J., Hutton, S., Rhodes, M.J., 2002. Effect of cohesive interparticle force on the flow characteristics of granular material. Powder Technol. 126, 150–154.
- Freeman, R., 2007. Measuring the flow properties of consolidated, conditioned and aerated powders a comparative study using a powder rheometer and a rotational shear cell. Powder Technol. 174, 25–33. https://doi.org/10.1016/j.powtec.2006.10.016
- Freyssingeas, E., Dalbe, M.J., Géminard, J.C., 2011. Flowers in flour: avalanches in cohesive granular matter. Phys. Rev. E 83, 167–177. https://doi.org/10.1103/PhysRevE.83.051307.
- Geldart, D., 1973. Types of gas fluidization. Powder Technol. 7, 285–292. https://doi.org/10.1016/0032-5910(73)80037-3.
- Geldart, D., Harnby, N., Wong, A.C., 1984. Fluidization of cohesive powders. Powder Technol. 37, 25–37. https://doi.org/10.1016/0032-5910(84)80003-0.
- Herminghaus, S., 2005. Dynamics of wet granular matter. Adv. Phys. 54, 221–261. https://doi.org/10.1080/00018730500167855.
- Hou, Q.F., Zhou, Z.Y., Yu, A.B., 2012. Micromechanical modeling and analysis of different flow regimes in gas fluidization. Chem. Eng. Sci. 84, 449–468. https:// doi.org/10.1016/j.ces.2012.08.051.
- Jaiswal, R.P., Kumar, G., Kilroy, C.M., Beaudoin, S.P., 2009. Modeling and validation of the van der waals force during the adhesion of nanoscale objects to rough surfaces: a detailed description. Langmuir 25, 10612–10623. https://doi.org/ 10.1021/la804275m.
- Jones, R., Pollock, H.M., Geldart, D., Verlinden, A., 2003. Inter-particle forces in cohesive powders studied by AFM: effects of relative humidity, particle size and wall adhesion. Powder Technol. 132, 196–210. https://doi.org/10.1016/S0032-5910(03)00072-X.
- Kunii, D., Levenspiel, O., 1991. Fluidization Engineering. Butterworth-Heinemann, Boston.
- LaMarche, C.Q., Leadley, S., Liu, P., Kellogg, K.M., Hrenya, C.M., 2017a. Method of quantifying surface roughness for accurate adhesive force predictions. Chem. Eng. Sci. 158, 140–153. https://doi.org/10.1016/j.ces.2016.09.024.
- LaMarche, C.Q., Liu, P., Kellogg, K.M., Hrenya, C.M., 2017b. Fluidized-bed measurements of carefully-characterized, mildly-cohesive (Group A) particles. Chem. Eng. J. 310, 259–271. https://doi.org/10.1016/j.cej.2016.10.119.
- LaMarche, C.Q., Liu, P., Kellogg, K.M., Weimer, A.W., Hrenya, C.M., 2015. A systemsize independent validation of CFD-DEM for noncohesive particles. AIChE J. 61, 4051–4058. https://doi.org/10.1002/aic.15057.
- 4051–4058. https://doi.org/10.1002/aic.15057.

  LaMarche, C.Q., Miller, A.W., Liu, P., Hrenya, C.M., 2016. Linking micro-scale predictions of capillary forces to macro-scale fluidization experiments in humid environments. AIChE J. https://doi.org/10.1002/aic.15281.
- Larson, I., Drummond, C.J., Chan, D.Y.C., Grieser, F., 1993. Direct force measurements between titanium dioxide surfaces. J. Am. Chem. Soc. 115, 11885–11890. https://doi.org/10.1021/ja00078a029.
- Leturia, M., Benali, M., Lagarde, S., Ronga, I., Saleh, K., 2014. Characterization of flow properties of cohesive powders: a comparative study of traditional and new testing methods. Powder Technol. 253, 406–423. https://doi.org/10.1016/j. powtec.2013.11.045.
- Li, T., Gopalakrishnan, P., Garg, R., Shahnam, M., 2012. CFD-DEM study of effect of bed thickness for bubbling fluidized beds. Particuology 10, 532-541. https:// doi.org/10.1016/j.partic.2012.02.006.
- Liu, P., Hrenya, C.M., 2018. Cluster-induced deagglomeration in dilute gravity-driven gas-solid flows of cohesive grains. Phys. Rev. Lett. 121, https://doi.org/10.1103/PhysRevLett. 121.238001 238001.
- Liu, P., Hrenya, C.M., 2014. Challenges of DEM: I. Competing bottlenecks in parallelization of gas-solid flows. Powder Technol. 264, 620–626. https://doi.org/10.1016/j.powtec.2014.04.095.
- Liu, P., LaMarche, C.Q., Kellogg, K.M., Hrenya, C.M., 2018. A square-force cohesion model and its extraction from bulk measurements. AIChE J. 82, 1156–1211. https://doi.org/10.1002/aic.16089.
- Liu, P., LaMarche, C.Q., Kellogg, K.M., Hrenya, C.M., 2016a. Fine-particle defluidization\_ interaction between cohesion, Young's modulus and static bed height. Chem. Eng. Sci. 145, 266–278. https://doi.org/10.1016/j.ces.2016.02.024.
- Liu, P., LaMarche, C.Q., Kellogg, K.M., Leadley, S., Hrenya, C.M., 2016b. Cohesive grains: bridging microlevel measurements to macrolevel flow behavior via surface roughness. AIChE J. 1–9. https://doi.org/10.1002/aic.15383.
- Liu, X., Xu, G., Gao, S., 2008. Micro fluidized beds: wall effect and operability. Chem. Eng. J. 137, 302–307. https://doi.org/10.1016/j.cej.2007.04.035.
- Loezos, P.N., Costamagna, P., Sundaresan, S., 2002. The role of contact stresses and wall friction on fluidization. Chem. Eng. Sci. 57, 5123–5141. https://doi.org/ 10.1016/S0009-2509(02)00421-9.
- Luding, S., 2005. Anisotropy in cohesive, frictional granular media. J. Phys.: Condens. Matt. 17, S2623–S2640. https://doi.org/10.1088/0953-8984/17/24/017.
- McCarthy, J.J., 2003. Micro-modeling of cohesive mixing processes. Powder Technol. 138, 63–67. https://doi.org/10.1016/j.powtec.2003.08.042.

- McMillan, J., Shaffer, F., Gopalan, B., Chew, J.W., Hrenya, C., Hays, R., Karri, S.B.R., Cocco, R., 2013. Particle cluster dynamics during fluidization. Chem. Eng. Sci. 100, 39–51. https://doi.org/10.1016/j.ces.2013.02.047.
- Mikami, T., Kamiya, H., Horio, M., 1998. Numerical simulation of cohesive powder behavior in a fluidized bed. Chem. Eng. Sci. 53, 1927–1940. https://doi.org/10.1016/S0009-2509(97)00325-4.
- Mitarai, N., Nori, F., 2007. Wet granular materials. Adv. Phys. 55, 1–45. https://doi.org/10.1080/00018730600626065.
- Molerus, O., 1982. Interpretation of Geldart's type A, B, C and D powders by taking into account interparticle cohesion forces. Powder Technol. 33, 81–87. https://doi.org/10.1016/0032-5910(82)85041-9.
- Müller, C.R., Holland, D.J., Sederman, A.J., Scott, S.A., Dennis, J.S., Gladden, L.F., 2008. Granular temperature: comparison of magnetic resonance measurements with discrete element model simulations. Powder Technol. 184, 241–253. https:// doi.org/10.1016/j.powtec.2007.11.046.
- Rabinovich, Y.I., Adler, J.J., Ata, A., Singh, R.K., Moudgil, B.M., 2000a. Adhesion between nanoscale rough surfaces. J. Colloid Interface Sci. 232, 10–16. https:// doi.org/10.1006/jcis.2000.7167.
- Rabinovich, Y.I., Adler, J.J., Ata, A., Singh, R.K., Moudgil, B.M., 2000b. Adhesion between nanoscale rough surfaces. J. Colloid Interface Sci. 232, 17–24. https:// doi.org/10.1006/jcis.2000.7168.
- Rhodes, M.J., Wang, X.S., Nguyen, M., Stewart, P., Liffman, K., 2001. Use of discrete element method simulation in studying fluidization characteristics: influence of interparticle force. Chem. Eng. Sci. 56, 69–76.
- Rhodes, M.J., 2008. Introduction to particle technology. John Wiley & Sons.
- Rognon, P.G., Roux, J.N., Wolf, D., Naaïm, M., Chevoir, F., 2007. Rheophysics of cohesive granular materials. EPL 74, 644–650. https://doi.org/10.1209/epl/ i2005-10578-v.
- Rumpf, H., 1990. Particle technology.
- Salehi, H., Barletta, D., Poletto, M., 2017a. A comparison between powder flow property testers. Particuology 32, 10–20. https://doi.org/10.1016/j.partic. 2016.08.003
- Salehi, H., Barletta, D., Poletto, M., Schütz, D., Romirer, R., 2017b. On the use of a powder rheometer to characterize the powder flowability at low consolidation with torque resistances. AIChE J. 63, 4788–4798. https://doi.org/10.1002/ aic.15934.
- Salehi, H., Sofia, D., Schütz, D., Barletta, D., Poletto, M., 2018. Experiments and simulation of torque in Anton Paar powder cell. Part. Sci. Technol. 36, 501–512. https://doi.org/10.1080/02726351.2017.1409850.
- Seville, J.P.K., Willett, C.D., Knight, P.C., 2000. Interparticle forces in fluidisation: a review. Powder Technol. 113, 261–268. https://doi.org/10.1016/S0032-5910 (00)00309-0.
- Shabanian, J., Chaouki, J., 2015. Hydrodynamics of a gas-solid fluidized bed with thermally induced interparticle forces. Chem. Eng. J. 259, 135–152. https://doi.org/10.1016/j.cej.2014.07.117.
- Srivastava, A., Sundaresan, S., 2002. Role of wall friction in fluidization and standpipe flow. Powder Technol. 124, 45–54.
- Stevens, A.B., Hrenya, C.M., 2005. Comparison of soft-sphere models to measurements of collision properties during normal impacts. Powder Technol. 154, 99–109. https://doi.org/10.1016/j.powtec.2005.04.033.
- Tegzes, P., Vicsek, T., Schiffer, P., 2002. Avalanche dynamics in wet granular materials. Phys. Rev. Lett. 89, 245–254. https://doi.org/10.1103/PhysRevLett. 89.094301.
- Tomas, J., 2004. Product design of cohesive powders-mechanical properties, compression and flow behavior. Chem. Eng. Technol.: Ind. Chem.-Plant Equip.-Process Eng.-Biotechnol. 27, 605–618.
- Tsinontides, S.C., Jackson, R., 2006. The mechanics of gas fluidized beds with an interval of stable fluidization. J. Fluid Mech. 255, 237–238. https://doi.org/10.1017/S0022112093002472.
- Valverde, J.M., Castellanos, A., 2007. Random loose packing of cohesive granular materials. EPL 75, 985–991. https://doi.org/10.1209/epl/i2006-10208-4.
- Valverde, J.M., Castellanos, A., Mills, P., Quintanilla, M.A.S., 2003. Effect of particle size and interparticle force on the fluidization behavior of gas-fluidized beds. Phys. Rev. E 67, 285–286. https://doi.org/10.1103/PhysRevE.67.051305.
- Visser, J., 1989. Van der Waals and other cohesive forces affecting powder fluidization. Powder Technol. 58, 1–10. https://doi.org/10.1016/0032-5910(89) 80001-4
- Wang, Z., Kwauk, M., Li, H., 1998. Fluidization of fine particles. Chem. Eng. Sci. 53, 377–395. https://doi.org/10.1016/S0009-2509(97)00280-7.
- Xu, Y., Li, T., Musser, J., Liu, X., Xu, G., Rogers, W.A., 2017. CFD-DEM modeling the effect of column size and bed height on minimum fluidization velocity in micro fluidized beds with Geldart B particles. Powder Technol. 318, 321–328. https:// doi.org/10.1016/j.powtec.2017.06.020.
- Yang, R.Y., Zou, R.P., Yu, A.B., 2003. Effect of material properties on the packing of fine particles. J. Appl. Phys. 94, 3025–3034. https://doi.org/10.1063/1.1598638.